Carbon 173 (2021) 565–571

Contents lists available at ScienceDirect

Carbon

journal homepage: www.elsevier.com/locate/carbon

Research Article

Gate controllable optical spin current generation in zigzag graphene nanoribbon

Liwen Zhang [a, d], Jun Chen [b, d, **], Lei Zhang [a, d, *], Fuming Xu [c], Liantuan Xiao [a, d], Suotang Jia [a, d]

[a] State Key Laboratory of Quantum Optics and Quantum Optics Devices, Institute of Laser Spectroscopy, Shanxi University, Taiyuan, 030006, China
[b] State Key Laboratory of Quantum Optics and Quantum Optics Devices, Institute of Theoretical Physics, Shanxi University, Taiyuan, 030006, China
[c] College of Physics and Optoelectronic Engineering, Shenzhen University, Shenzhen, 518060, China
[d] Collaborative Innovation Center of Extreme Optics, Shanxi University, Taiyuan, 030006, China

ARTICLE INFO

Article history:
Received 25 August 2020
Received in revised form
2 November 2020
Accepted 9 November 2020
Available online 17 November 2020

ABSTRACT

Considering the demand for long spin communication distance in spintronics, graphene presents micrometer spin relaxation length at room temperature, making it one of the most promising two dimensional spintronic materials. However, achieving efficient spin injection (including pure spin current and spin polarized current) by reducing the spin dependent scattering between graphene and other materials like contact is still a core challenge. Here, we propose a novel approach to generate spin current in zigzag graphene nanoribbon (ZGNR) via photogalvanic (or photovoltaic) effect (PGE) from atomic first principle calculations. By designing ZGNR based device with spatial inversion symmetry, we find that the PGE induced pure spin current can be hiddenly generated without accompanying charge current. Furthermore, through applying a dual gate in the system, the generated pure spin current can be controlled when dual gate voltages have the opposite signs. Interestingly, when the signs of dual gate voltages are the same, the pure spin current can turn into the fully spin polarized current. More importantly, the generated spin current via PGE is independent of photon polarization and incident angles. Our investigations demonstrate ZGNR's great potential application in noninvasive spin injection of the graphene based spintronic device.

1. Introduction

Nowadays, the continuous scaling down of traditional complementary metal-oxide-semiconductor (CMOS) faces a great challenge [1,2]. On the one hand, the cost of chips is largely increased because of the required advanced facilities in the fabrication process. On the other hand, the transistor size is approaching the limit where quantum effect plays an important role. For instance, the increase of gate leakage current due to the quantum tunneling effect which in turn increases the stand by power dissipation. However, the rapid growth of the Internet of Things and big data are still in high demand for much lower power and faster speed in data process and storage. Therefore, people are resorting to other technologies beyond CMOS technology.

As one of the most promising ultra-fast and low-power consumption devices, spintronics aims to utilize the spin degree of freedom as the information carrier instead of charge itself [3]. At present, many spintronic devices with different functionalities have been developed, for instance, giant magnetoresistance, spin valve and so on [4–8]. However, it is still lacking an ideal material that can transport spin information over long distances even at room temperature. Since the discovery of graphene, two dimensional materials become an important material platform in spintronics [9–15]. As one of the most promising spintronic materials, graphene has very high mobility, negligible hyperfine interaction, and especially extremely small spin-orbital coupling strength [16–19]. It is experimentally shown that the spin relaxation length of graphene can be as long as $\sim 30\ \mu$m at room temperature and several

* Corresponding author. State Key Laboratory of Quantum Optics and Quantum Optics Devices, Institute of Laser Spectroscopy, Shanxi University, Taiyuan, 030006, China.
** Corresponding author. State Key Laboratory of Quantum Optics and Quantum Optics Devices, Institute of Theoretical Physics, Shanxi University, Taiyuan, 030006, China.
E-mail addresses: chenjun@sxu.edu.cn (J. Chen), zhanglei@sxu.edu.cn (L. Zhang).

https://doi.org/10.1016/j.carbon.2020.11.033
0008-6223/

graphene devices have been demonstrated experimentally [20–23]. This unique property enables the realistic transportation and manipulation of spin information in graphene based complex device structures [22–25]. It is commonly accepted that, the generation of spin is of central importance in spintronics. At present, the spins can be injected from ferromagnetic (FM) metal into graphene. Due to the presence of an interface between FM and graphene, the spin dependent scattering may cause the low spin injection efficiency [16,26–28]. By combining h-BN and topological semimetal WTe_2 and graphene, the spin injection efficiency has been enhanced [29–31]. Moreover, people are developing the nondestructive optical spin injection approaches. However, it is also a challenge due to the lack of spin dependent optical selection rules and weak optical absorption in pristine graphene [32]. More recently, it is found that the photo-excited spin polarized carrier in monolayer transition metal dichalcogenides (TMDs) can be diffused into graphene via proximity coupling effect [31–36]. It is well known, one of the central tasks in spintronics is to achieve large spin polarization and the ultimate goal is to use pure spin current without accompanying charge current [37]. Thus, following questions arise naturally: is it possible to efficiently inject the spin current (including both fully spin polarized current and pure spin current) without coupling graphene with other materials? If so, can the generated spin current be further controlled conveniently?

In this letter, we propose a novel approach to generate spin current in zigzag graphene nanoribbon (ZGNR) via photogalvanic effect (PGE) or photovaltic effect instead of using proximity coupling effect between graphene and other materials. Based on non-equilibrium Green's function (NEGF) combined with density functional theory (DFT), we find that the pure spin current can be produced in pristine ZGNR when linearly polarized or circularly polarized light is illuminated. More importantly, the pure spin current can be obtained in a wide range of photon energy and independent of photon polarization and incident angles. Through applying the dual gate voltages in the ZGNR, the magnitude and sign of pure spin current can be both controlled. When the photon energy is fixed, the generated pure spin current can be turned on and off. More importantly, the fully spin polarized current can also be produced by changing the relative signs of the dual gate voltages.

2. Model and theoretical formalism

Firstly, the atomic structures of ZGNR with different widths are fully relaxed until the residual force on each atom is smaller than 0.001 eV/Å by using Vienna *ab initio* simulation package (VASP) [38,39]. In the numerical calculation, the kinetic energy cutoff is chosen as 520 eV and $10 \times 1 \times 1$ *k*-point mesh is chosen for the first Brillouin-zone integration [40]. The exchange-correlation potential is taken as the generalized gradient approximation (GGA) with the Perdew-Burke-Ernzerhof (PBE) form [41]. To avoid the interaction between repeated images, the vacuum space along *y* and *z* directions are chosen to be larger than 16 Å and 15 Å, respectively. Based on the optimized atomic structures, quantum transport calculations are carried out based on non-equilibrium Green's function (NEGF) combined with density functional theory (DFT) formalism [42–44], as implemented in the Nanodcal transport package [44]. In the self-consistent simulation, the physical quantities are expanded with the linear combination of atomic orbital (LCAO) basis at the double-ς polarization (DZP) level; the atomic cores are described by the standard norm-conserving nonlocal pseudo-potentials [45]; the local density approximation is applied for the exchange-correlation potential. The *k*-point mesh is adopted as $100 \times 1 \times 1$ for the self-consistent calculation of lead regions. The self-consistency is deemed as achieved until the monitored quantities such as every element of the Hamiltonian and density matrices differ less than 1×10^{-8} a.u. between iteration steps.

Fig. 1 shows the schematic plot of a two-probe device structure based on ZGNR. Note that dual transverse gates are applied in the system to tune the generated spin current with PGE. The linearly or circularly polarized light is shining on the central scattering region (the region of length *L*). In the following, we shall only consider the spin current flowing into the left lead. The spin dependent photocurrent $J_{L,s}^{(ph)}$ can be expressed as [46–49]:

$$J_{L,s}^{(ph)} = \frac{ie}{h}\int \mathrm{Tr}\left\{\Gamma_L\left[G_{ph}^{<} + f_L(E)\left(G_{ph}^{>} - G_{ph}^{<}\right)\right]\right\}_{ss} dE, \tag{1}$$

where *L* indicates the left lead and *s* indicates the spin component ($s = \uparrow, \downarrow$); *e* and *h* are the electron charge and the Plank's constant; $\Gamma_L = i(\Sigma_L^r - \Sigma_L^a)$ is the linewidth function and $\Sigma_L^r = [\Sigma_L^a]^\dagger$ is the retarded self-energy due to the presence of the left lead; $G_{ph}^{<\,/\,>} = G_0^r \Sigma_{ph}^{<\,/\,>} G_0^a$ represents the lesser/greater Green's function including electron-photon interaction [50], where the $G_0^{r/a}$ is the retarded/advanded Green's functions without photons; $f_L(E)$ is the Fermi-Dirac distribution function of the left lead. The polarization of the light can be defined by a complex vector **e**. The corresponding unit vectors $\mathbf{e}_1$ and $\mathbf{e}_2$ are in the *x* and -*y* directions respectively [as shown in Fig. 1 (a)]. For a linearly polarized light, $\mathbf{e} = \cos\theta\mathbf{e}_1 + \sin\theta\mathbf{e}_2$. For an elliptically polarized light, $\mathbf{e} = \cos\varphi\mathbf{e}_1 \pm i\sin\varphi\mathbf{e}_2$ [48]. For simplicity, we introduce a normalized photocurrent [47,50], i.e. spin related photoresponse R_s,

$$R_s = \frac{J_{L,s}^{(ph)}}{eI_\omega}, \tag{2}$$

where the unit of R_s is $a_0^2/photon$ and a_0 represents the Bohr radius; $J_{L,s}^{(ph)}$ is the spin related photocurrent defined in Eq. (1); *e* is the electron charge; I_ω is the photon flux defined as the number of photons per unit time per unit area. Thus, the charge current and spin current can be defined as

$$\begin{aligned} I_c &= R_\uparrow + R_\downarrow, \\ I_s &= R_\uparrow - R_\downarrow. \end{aligned} \tag{3}$$

Here, the $R_{\uparrow/\downarrow}$ represents the photoresponse with spin up or spin down component. Furthermore, the spin polarization (*SP*) is introduced

$$SP(\%) = \frac{||R_\uparrow| - |R_\downarrow||}{|R_\uparrow| + |R_\downarrow|} \times 100. \tag{4}$$

3. Results and discussion

In the beginning, we investigate the bulk electronic properties of ZGNR. Since the width of the ZGNR can be classified by the number of zigzag chains along the *y* direction, we refer to the ZGNR as *n*-ZGNR in the following (here, we mainly take 5-ZGNR as an example to analysis (if not specified)). The band structure of 5-ZGNR is shown in the left column of Fig. 2(a). It is clear that the spin up and spin down bands are degenerate. By calculating the spin density $\rho_s = \rho_\uparrow - \rho_\downarrow$ [right column in Fig. 2(a)], we can know that the charge density of spin up and down components mainly distribute at the upper and lower edges, which indicates that ZGNR is in the antiferromagnetic insulating ground state. When the external transverse gate voltage is applied [shown in Fig. 2(d)], the spin up and down bands split as

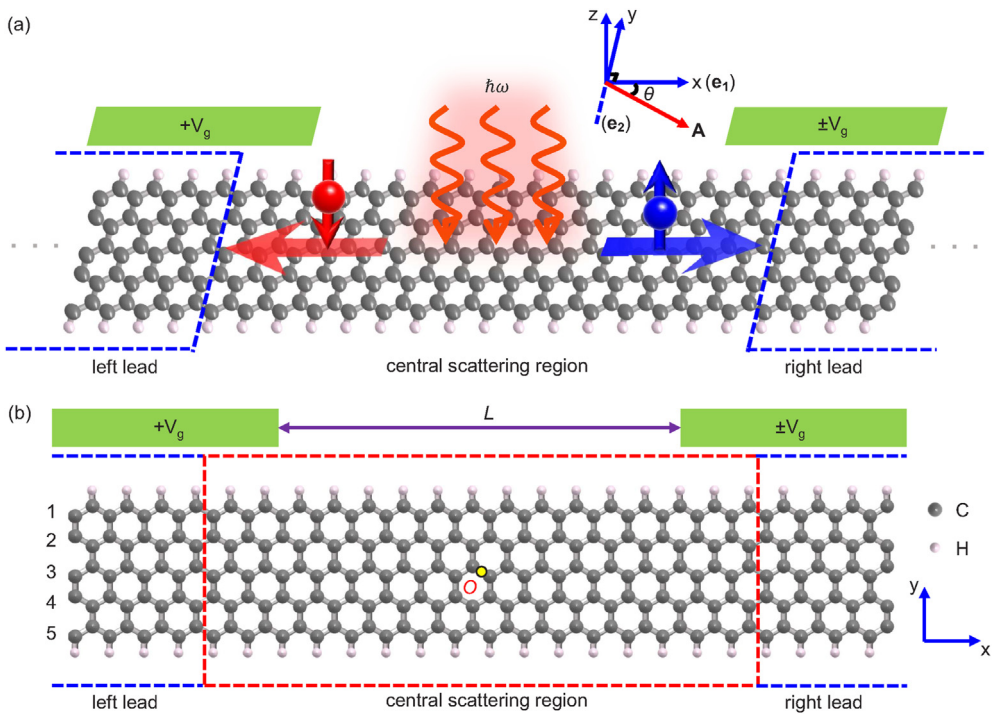

Fig. 1. Schematic plot of a two-probe device structure constructed by the ZGNR with a dual transverse gate. (a) Side view; (b) Top view. The gate voltage applied to the left lead is fixed at $+V_g$ while the gate voltage exerted on the right lead can be $\pm V_g$. The light is shining in the central scattering region. The red and blue balls with downward and upward arrows schematically represent the flow of the spin down and spin up electrons excited to the conduction band in PN configuration, respectively. Here, **A** is the electromagnetic vector potential inside the *x-y* plane. $\mathbf{e}_1$ and $\mathbf{e}_2$ are two unit vectors for characterizing the polarization of the light. θ denotes the polarization angle of the linearly polarized light. L is the length of the illuminated region. Gray and pink spheres denote carbon and hydrogen atoms, respectively. O is the inversion center point of the whole device. (A colour version of this figure can be viewed online.)

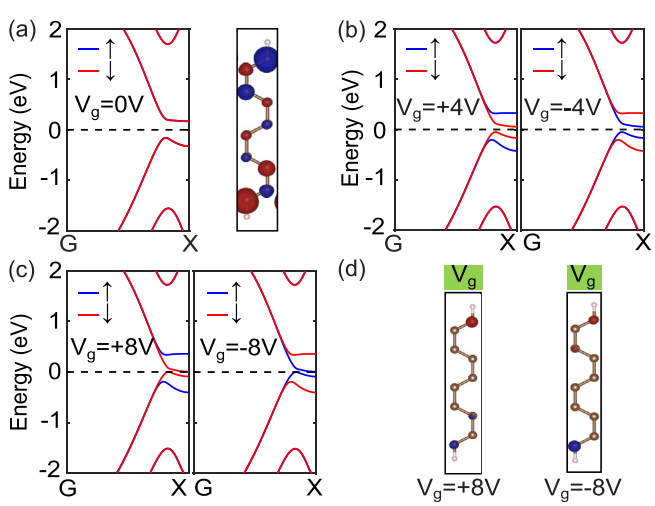

Fig. 2. (a) Band structure and the spatial distribution of spin density ρ_s of 5-ZGNR. Blue and red areas in the right column denote positive and negative values, respectively. (b–c) Band structures of bulk 5-ZGNR with $V_g = \pm 4$ V, ± 8 V. (d) Spin density difference $\Delta\rho_s = \rho_s(V_g = \pm 8V) - \rho_s(V_g = 0V)$ in the left and right column, respectively. The transverse gate voltage is applied in the green region. Note that the isosurface value of spin-charge density in (a) and (d) are set as 0.0002. (A colour version of this figure can be viewed online.)

shown in Fig. 2(b and c). Furthermore, the spin up band gap increases/decreases while the spin down band gap decreases/increases when the gate voltage is positive/negative. As the gate voltage is further increased, the band gap closes and ZGNR becomes halfmetal in Fig. 2(c). In Fig. 2(d), the changes of spin density induced by gate voltages $\Delta\rho_s = \rho_s(V_g = \pm 8V) - \rho_s(V_g = 0V)$ are presented. Physically, it is known that both the spin up and spin down charge densities move upward/downward under a positive/negative gate voltage. As shown in Fig. 2 (d), we can know that the spin density difference is positive/negative in the lower/upper edge regardless of the gate voltages sign. However, for the positive case (left column in Fig. 2(d)), the magnitude of the negative part in the upper edge is larger than that of the negative part in the lower edge, which means the increase of spin density in the upper edge is larger than the decrease of spin density in the lower edge. This is different for the negative case. From the right column in Fig. 2(d), it is found that the increase of spin density in the upper edge is smaller than the decrease of spin density in the lower edge. This means that the transverse gate can be used as an effective tool to tune the spin dependent electronic property of ZGNR [51,52]. The spin-dependent bandgap versus the gate voltage for n-ZGNR ($n = 3,5,7,9$) are presented in Supplement Information (Fig. S1). Based on these unique properties of the ZGNR, we construct a ZGNR based two-probe devices with dual gates as shown in Fig. 1(a). Note that the device structure holds inversion symmetry with a inversion center shown in Fig. 1(b). During the numerical simulation, the device can be divided into three parts as shown in Fig. 1(b): the central scattering region and left/right lead which extends to infinity. Here, the light (linearly polarized or circularly polarized) is vertically illuminated in the central scattering region. In the following, the left gate voltage is fixed as positive, while that exerted on the right lead can be switched. For convenience, the positive-positive and positive-negative gate voltages in the dual gate are denoted by PP and PN in the following, respectively.

We now analyze the spin current generated by linearly polarized photogalvanic effect (LPGE) and circularly polarized photogalvanic effect (CPGE). As shown in Fig. 3(a), the pure spin current is

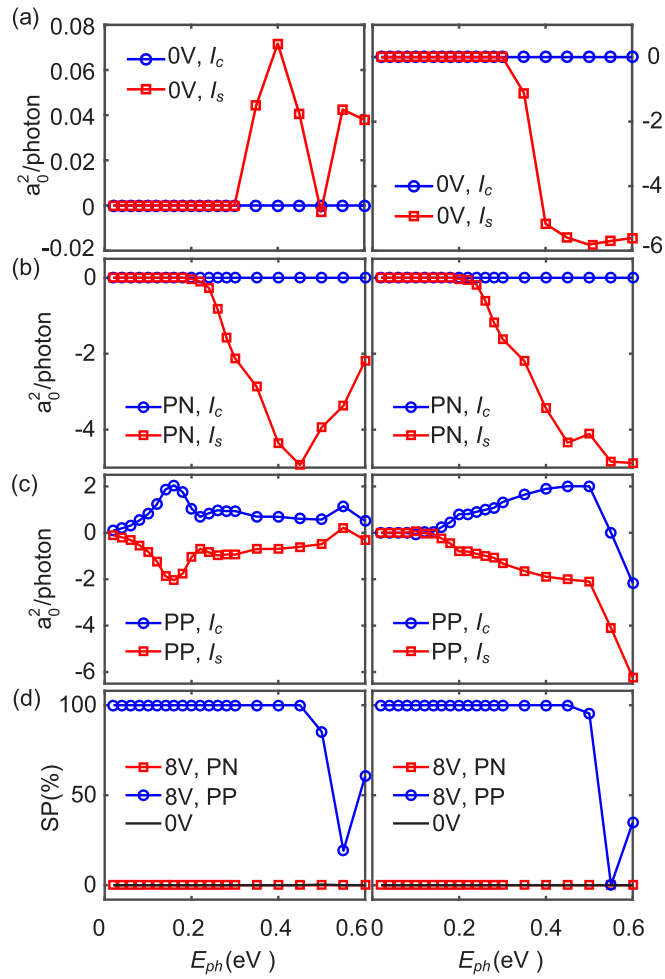

Fig. 3. Charge current (I_c), spin current (I_s) and spin polarization [SP (%)] versus photon energy (E_{ph}) generated by LPGE (left column) and CPGE (right column). (a) Charge current (I_c) and spin current (I_s) when $V_g = 0$. (b,c) Charge current (I_c) and spin current (I_s) in PN and PP configurations, respectively. Here the gate voltage V_g is equal to 8 V. (d) Spin polarization for $V_g = 0$ V (black solid line), PN (red hollow square line) and PP (blue hollow circle line) configurations. Note that the photon polarization angles are $\theta = 45^\circ$, $\varphi = 45^\circ$ for LPGE and CPGE, respectively. (A colour version of this figure can be viewed online.)

produced for both LPGE and CPGE in ZGNR without applying the gate voltage ($V_g = 0$ V). Since the device structure maintains spatial inversion symmetry, the charge current can not be generated by PGE. This is consistent with phenomenological theory [53]. However, the pure spin current can still be obtained if the spin density has no spatial inversion symmetry regardless of light's polarization and its incident angle [54,55]. As shown in Fig. 2(a), the charge density with spin up or down component are distributed in upper or lower edge, respectively. Thus, the spin density is anti-symmetrically distributed [$\rho_\uparrow(\mathbf{r}) = \rho_\downarrow(-\mathbf{r})$] and thus it is an anti-ferromagnetic coupling between any two atoms with respect to the inversion center. Compared with LPGE, the pure spin current is also obtained via CPGE while their magnitudes are much larger. By analyzing the effective transmission (shown in Fig. S2 in SI), we can find that the transport probabilities of outgoing electrons in CPGE are much larger than that of incoming electrons in CPGE resulting in a relatively large pure spin current when Vg = 0 V. In order to know the gate voltage effect, the numerical results of spin current generated in PN and PP configurations when $V_g = 8$ V are presented in Fig. 3(b and c). In PN configuration, the pure spin current can be induced when the photon energy is larger than 0.2 eV. This indicates that the pure spin current can be tuned by adjusting the gate voltage. Interestingly, the magnitude of pure spin current with LPGE is largely increased compared with zero gate voltage case (the maximum magnification factor can be as large as $\sim 10^5$). This can be understood by analyzing the effective transmission shown in the first section of the Supplementary Information. While in CPGE, the magnitude of pure spin current does not change too much when the gate voltage is applied. Accordingly, the spin polarization of the PN configuration is always equal to zero in the given photon energy range shown in Fig. 3(d). In PP configuration, the spin density is no longer anti-symmetrically distributed [$\rho_\uparrow(\mathbf{r}) \neq \rho_\downarrow(-\mathbf{r})$], which can be estimated from the spin density difference shown in left column of Fig. 2(d). From Fig. 3(c), we can easily find that the spin polarized current is generated with LPGE and CPGE, since the accompanying charge current is generated. Interestingly, the charge current and spin current have equal magnitude and opposite signs in a wide range of photon energies (the photon energy is less than 0.45 eV), which means $I_s + I_c = 2R_\uparrow = 0$ and the fully spin polarized current with spin down component is produced. Correspondingly, the spin polarization of PP configuration is 100% when the photon energy is less than 0.45 eV as shown in Fig. 3(d). Therefore, by tuning the dual gate voltages, the pure spin current and fully spin polarized current can both be generated in our proposed device. Moreover, the sign of pure spin current can be changed and fully spin polarized current with different spin component can be obtained by tuning the sign of dual gate voltages (See more numerical results in section II of the Supplementary Information).

To further understand the physics behind the generation of spin current, we take LPGE in PN configuration as an example to give a physical picture. In the first place, the local density of states (LDOS) of the central scattering region is presented in Fig. 4(a). Due to the presence of positive and negative gate voltages exerted on the left and right sides of the central region, the spin down and up band gap close correspondingly in these two regions and they still keep open in the other regions. In the light illumination region [between the two pink vertical lines shown in Fig. 4(a)], the valence band of spin up and down components gradually bend upward and downward, respectively, while the situation is reversed for the conduction band. Fig. 4(b) presents a qualitative physical picture of the generation of pure spin current, which can be divided into three processes. Firstly, the electron below the Fermi level with energy ε_{in} can be excited into states with energy $\varepsilon_{out} = \varepsilon_{in} + E_{ph}$ by absorbing incident photons ($E_{ph} = \hbar\omega$) in the central scattering region. From LDOS shown in Fig. 4(a), we can know that both spin up and down states with energies $-0.4eV < \varepsilon_{in} < 0$ are available to be excited. Secondly, the excited electrons will flow out of the central scattering region into the leads. It is worth mentioning that the excited electrons with spin up component can only flow into the right lead when the photon energy is not too large, since there is no available spin up states (with finite band gap) in the left lead [see Fig. 4(a)]. At the same time, the excited electrons with spin down component can only flow into left lead, since there is no available spin down states (with finite band gap) in the right lead. Thus, the minimum required photon energy to generate spin current is determined by the energy gap E_{g1} shown in Fig. 4(a and b). Thirdly, the electrons with energy ε_{in} in the leads flow into the central scattering region to fill the holes left during the excitation process. Due to the presence of the spatial inversion symmetry, which means motion of incoming and outgoing electrons will cancel each other resulting in zero charge current. However, the hidden net spin flow can still be produced during this process. By rewriting Eq. (1) (where we have assumed that the temperature is low enough and the Fermi

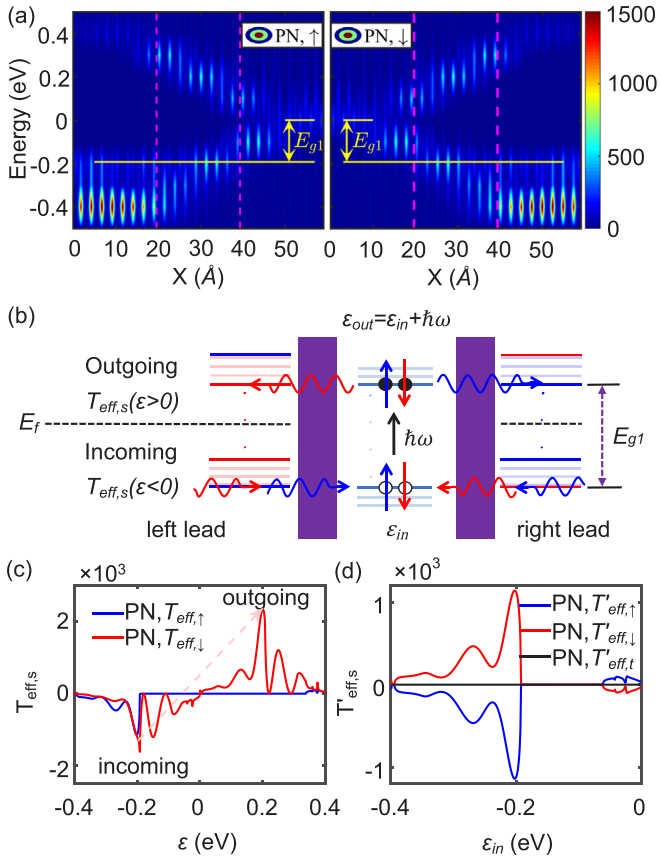

Fig. 4. (a) The local density of states (LDOS) of spin up (left column) and spin down (right column) components versus electron energy and transport direction (x). The light illumination region is between the two pink vertical lines. Physical process of the generation of the pure spin current in PN configuration is schematically plotted in (b). Here blue/red lines denote motion of spin up/down electrons, respectively. Wiggle lines denote motion of incoming and outgoing electrons. The Fermi level $E_f = 0$. (c) The effective transmission $T_{eff,s}$ versus electron energy ε. (d) The net effective transmission $T'_{eff,s}$ versus electron energy ε_{in}. Here, the gate voltage $V_g = 8$ V is applied and the system is irradiated by a linearly polarized light with $E_{ph} = 0.4$ eV. (A colour version of this figure can be viewed online.)

function $f_L(\varepsilon)$ is stepwise) [49], we can split the spin dependent current into incoming and outgoing terms

$$J_{L,s}^{(ph)} = \frac{ie}{h}\left\{\int_{-\infty}^{0} \mathrm{Tr}\left[\Gamma_L G_{ph}^{>}\right]_{ss} d\varepsilon + \int_{0}^{\infty} \mathrm{Tr}\left[\Gamma_L G_{ph}^{<}\right]_{ss} d\varepsilon\right\}. \quad (5)$$

Furthermore, the incoming effective transmission $T_{eff,s}(\varepsilon<0) = \mathrm{Tr}[\Gamma_L G_{ph}^{>}]_{ss}$ and outgoing effective transmission $T_{eff,s}(\varepsilon>0) = \mathrm{Tr}[\Gamma_L G_{ph}^{<}]_{ss}$ can be introduced in order to analyze the electron transport process. As an example, the effective transmission with photon energy $E_{ph} = 0.4$ eV and $V_g = 8$ V is shown in Fig. 4(c). It is found that the $T_{eff,\uparrow}$ is mainly nonzero when $\varepsilon < -0.2$ eV. Compared with $T_{eff,\uparrow}$, $T_{eff,\downarrow}$ is nonzero in both incoming and outgoing regions, which is consistent with above analysis. For each spin channel s, the net effective transmission function is $T'_{eff,s}(\varepsilon_{in}) = T_{eff,s}(\varepsilon_{in}) + T_{eff,s}(\varepsilon_{in} + E_{ph})$, where $\varepsilon_{in} < 0$. From Eq. (5), the integration of $T'_{eff,s}(\varepsilon_{in})$ over ε_{in} gives the spin dependent current. As shown in Fig. 4(d), we can clearly see that $T'_{eff,\uparrow}(\varepsilon_{in}) = -T'_{eff,\downarrow}(\varepsilon_{in})$ and the total effective charge transmission $T'_{eff,t} = T'_{eff,\uparrow} + T'_{eff,\downarrow} = 0$. However, the effective spin transmission is nonzero, since we have $T'_{eff,t,s} = T'_{eff,\uparrow} - T'_{eff,\downarrow} \neq 0$, which indicates that the pure spin current can be obtained. The similar analysis on fully spin polarized current generated in PP configuration is presented in section III of the Supplementary Information.

Having understood the physical picture of pure spin current generation, we now calculate the spin current versus the photon polarization angles by fixing the photon energy $E_{ph} = 0.4$ eV. We consider PN and PP configurations with LPGE by varying θ and CPGE by varying φ, respectively. Fig. 5(a and b) plot the calculated spin current versus θ and φ. In PN configuration, the pure spin current without accompanying charge current is generated and independent of polarization angles both in LPGE and CPGE cases. In PP configuration, the magnitudes of charge current and spin current are equal to each other but with opposite signs, i.e., $I_c + I_s = 2R_\uparrow = 0$. Thus, only the current with the spin down component is obtained, which is also independent of photon polarization angles. More importantly, the magnitudes of pure spin current in PN and fully spin polarized current in PP can be largely tuned via photon polarization angles. Actually, the pure spin current and fully spin polarized current are also independent of photon incident angles (see more numerical results in the fourth section of the Supplementary Information).

Last but not the least, we study the effect of gate voltage and ZGNR's width in producing the pure spin current in PN configuration. To illustrate it, the phase diagram of pure spin current versus photon energy E_{ph} and gate voltage V_g is shown in Fig. 6(a). It is clear that the pure spin current can be generated in a wide range of parameter space (E_{ph}, V_g). Moreover, the required minimum photon energies E_{ph} to generate pure spin current at different gate voltages are also marked using a black dotted line in Fig. 6(a). This indicates

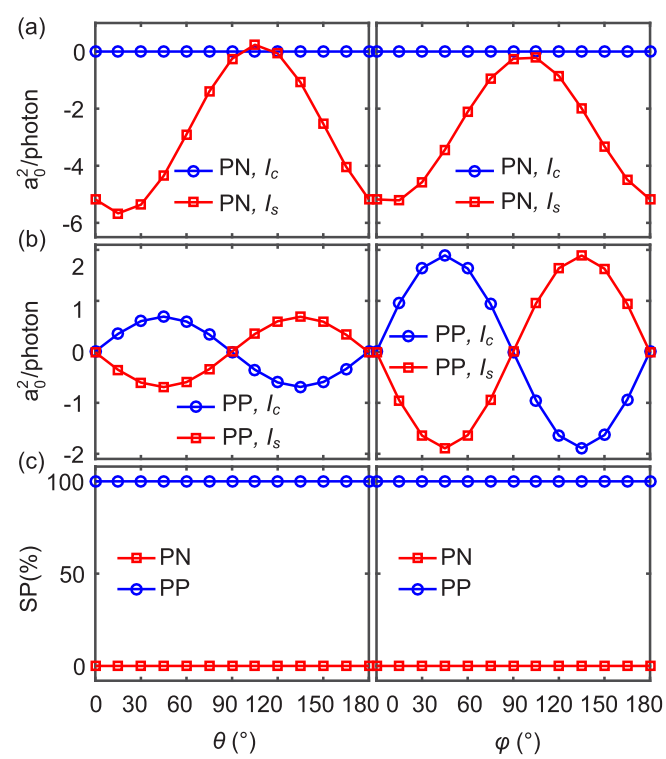

Fig. 5. Charge current (I_c) and spin current (I_s) versus polarization angle θ with LPGE (left column) and φ with CPGE (right column), respectively. (a) PN configuration. (b) PP configuration. The blue hollow circle line and the red hollow square line represent charge current and spin current, respectively. (c) Spin polarization [SP (%)] versus θ and φ for PN and PP configurations. Here the photon energy and gate voltage is fixed as $E_{ph} = 0.4$ eV, $V_g = 8$ V. (A colour version of this figure can be viewed online.)

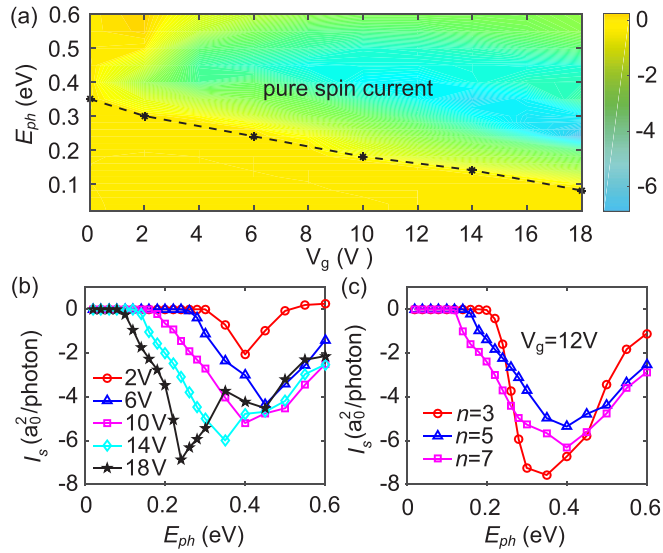

Fig. 6. (a) Phase diagram of pure spin current versus photon energy (E_{ph}) and gate voltages (V_g) of 5-ZGNR based device. The black dotted line represents the minimum photon energy at different gate voltages to generate pure spin current. (b) Pure spin current (I_s) of PN configuration versus photon energy E_{ph} under different gate voltages V_g in 5-ZGNR based device. (c) Pure spin current of PN configuration versus photon energy under different ribbon widths (n) when the gate voltage $V_g = 12$ V. Here, the polarization angle θ with LPGE is equal to 45°. (A colour version of this figure can be viewed online.)

that the pure spin current can be turned off by either tuning the photon energy or gate voltage in the system. As shown in Fig. 6(b), we find that the photon energy range of generating nonzero pure spin current gradually increases with the increasing gate voltage. In addition, the pure spin current can also be obtained in other ZGNR systems [see Fig. 6(c)], which presents a similar trend. Note that the minimum photon energy of generating pure spin current also decreases with the increase of the ribbon width due to the decreasing band gap of the corresponding system.

4. Conclusion

In summary, we theoretically propose a novel spin current injection approach into graphene. Here, the pure spin current and fully spin polarized current can be obtained and controlled via PGE by applying a dual gate in ZGNR based device. When the system is in PN or PP configuration, the pure spin current or fully spin polarized current can be obtained in a wide range of parameter space (E_{ph},V_g). More importantly, the generated spin current can be largely tuned by the photon energy, polarization angles and gate voltages, which means that it can be effectively controlled. In addition, the photon energy range to produce spin current can be modulated by changing the gate voltage and nanoribbon's width. Since the proposed device can be easily contacted with different graphene based spintronic devices, our work provides a novel noninvasive spin current injection mechanism.

CRediT authorship contribution statement

Liwen Zhang: Numerical Simulation, Visualization, Design the project, Supervision, Writing – original draft. **Jun Chen:** Design the project, Supervision, Writing – original draft. **Lei Zhang:** Writing – review & editing. **Fuming Xu:** Visualization, Writing – review & editing.

Declaration of competing interest

The authors declare that they have no known competing financial interests or personal relationships that could have appeared to influence the work reported in this paper.

Acknowledgement

We also gratefully acknowledge the support from the National Natural Science Foundation of China (Grants No. 11704232, 11674204, 12074230), National Key R&D Program of China under Grants No. 2017YFA0304203, PCSIRT (No. IRT_17R70), Natural Science Foundation of Guangdong Province (No. 2020A1515011418), 1331KSC, Shanxi Province 100-Plan Talent Program. Li-Wen Zhang is grateful to Min Zhou for useful discussions. This research was conducted using the High Performance Computer of Shanxi University.

Appendix A. Supplementary data

Supplementary data to this article can be found online at https://doi.org/10.1016/j.carbon.2020.11.033.

References

[1] International Roadmap for Devices and Systems: beyond Cmos, IEEE..
[2] W.M. Mitchell, The chips are down for moore's law, Nature 530 (7589) (2016) 144–147.
[3] S.A. Wolf, D.D. Awschalom, R.A. Buhrman, J.M. Daughton, S. von Molnár, M.L. Roukes, A.Y. Chtchelkanova, D.M. Treger, Spintronics: a spin-based electronics vision for the future, Science 294 (5546) (2001) 1488–1495.
[4] Z.H. Xiong, D. Wu, Z.V. Vardeny, J. Shi, Giant magnetoresistance in organic spin-valves, Nature 427 (6977) (2004) 821–824.
[5] T. Song, X. Cai, W.Y.T. Matisse, X. Zhang, B. Huang, N.P. Wilson, K.L. Seyler, L. Zhu, T. Takashi, K. Watanabe, M.A. McGuire, D.H. Cobden, D. Xiao, W. Yao, X. Xu, Giant tunneling magnetoresistance in spin-filter van der waals heterostructures, Science 360 (6394) (2018) 1214–1218.
[6] S. Yuasa, T. Nagahama, A. Fukushima, Y. Suzuki, K. Ando, Giant room-temperature magnetoresistance in single-crystal fe/mgo/fe magnetic tunnel junctions, Nat. Mater. 3 (12) (2004) 868–871.
[7] B. Sabpreet, S. Rachid, H. Atsufumi, O. Hideo, F. Shunsuke, S.N Piramanayagam, Spintronics based random access memory: a review, Mater. Today 20 (9) (2017) 530–548.
[8] M. Zhou, H. Jin, Y. Xing, In-plane dual-gated spin-valve device based on the zigzag graphene nanoribbon, Phys. Rev. Applied 13 (2020), 044006.
[9] X. Lin, W. Yang, K. Wang, W. Zhao, Two-dimensional spintronics for low-power electronics, Nat. Electron. 2 (2019) 274–283.
[10] A. Avsar, H. Ochoa, F. Guinea, B. Özyilmaz, J. Van Wees, I.J. Veramarun, Colloquium: spintronics in graphene and other two-dimensional materials, Rev. Mod. Phys. 92 (2) (2020), 021003(28).
[11] I. Žutić, J. Fabian, S. Das Sarma, Spintronics: fundamentals and applications, Rev. Mod. Phys. 76 (2004) 323–410.
[12] H. Jin, J. Li, T. Wang, Y. Yu, Photoinduced pure spin-current in triangulene-based nano-devices, Carbon 137 (2018) 1–5.
[13] L. Zhang, J. Chen, X. Zheng, B. Wang, L. Zhang, L. Xiao, S. Jia, Gate-tunable large spin polarization in few-layer black phosphorus based spintronic device, Nanoscale 11 (2019) 11872–11878.
[14] X. Tao, L. Zhang, X. Zheng, H. Hao, X. Wang, L. Song, Z. Zeng, H. Guo, h-bn/graphene van der waals vertical heterostructure: a fully spin-polarized photocurrent generator, Nanoscale 10 (1) (2018) 174–183.
[15] L.L. Tao, K.T. Cheung, L. Zhang, J. Wang, All-electrical generation of spin-polarized currents in quantum spin hall insulators, Phys. Rev. B 95 (2017), 121407.
[16] N. Tombros, C. Jozsa, M. Popinciuc, H.T. Jonkman, B.J. Van Wees, Electronic spin transport and spin precession in single graphene layers at room temperature, Nature 448 (7153) (2007) 571–574.
[17] H. Wei, R. Kawakami, G. Martin, F. Jaroslav, Graphene spintronics, Nat. Nanotechnol. 9 (10) (2014) 794–807.
[18] A.K. Geim, K.S. Novoselov, The rise of graphene, Nat. Mater. 6 (3) (2007) 183–191.
[19] S. Dushenko, H. Ago, K. Kawahara, T. Tsuda, S. Kuwabata, T. Takenobu, T. Shinjo, Y. Ando, M. Shiraishi, Gate-tunable spin-charge conversion and the role of spin-orbit interaction in graphene, Phys. Rev. Lett. 116 (16) (2016), 166102.
[20] J. Ingla-Aynés, M.H.D. Guimarães, R.J. Meijerink, P.J. Zomer, B.J. van Wees, 24-μm spin relaxation length in boron nitride encapsulated bilayer graphene, Phys. Rev. B 92 (2015), 201410.

[21] M. Drögeler, C. Franzen, F. Volmer, T. Pohlmann, L. Banszerus, M. Wolter, K. Watanabe, T. Taniguchi, C. Stampfer, B. Beschoten, Spin lifetimes exceeding 12 ns in graphene nonlocal spin valve devices, Nano Lett. 16 (6) (2016) 3533–3539.
[22] D. Khokhriakov, B. Karpiak, A.M. Hoque, S.P. Dash, Two-dimensional spintronic circuit architectures on large scale graphene, Carbon 161 (2020) 892–899.
[23] Z.M. Gebeyehu, S. Parui, J.F. Sierra, M. Timmermans, M.J. Esplandiu, S. Brems, C. Huyghebaert, K. Garello, M.V. Costache, S.O. Valenzuela, Spin communication over 30 μm long channels of chemical vapor deposited graphene on sio2, 2D Mater. 6 (3) (2019), 034003.
[24] M.V. Kamalakar, C. Groenveld, A. Dankert, S.P. Dash, Long distance spin communication in chemical vapour deposited graphene, Nat. Commun. 6 (2015) 6766.
[25] X. Lin, L. Su, Z. Si, Y. Zhang, A. Bournel, Y. Zhang, J. Klein, A. Fert, W. Zhao, Gate-driven pure spin current in graphene, Phys. Rev. Applied 8 (3) (2017), 034006.
[26] G. Schmidt, D. Ferrand, L.W. Molenkamp, A.T. Filip, B.J. van Wees, Fundamental obstacle for electrical spin injection from a ferromagnetic metal into a diffusive semiconductor, Phys. Rev. B 62 (2000) R4790–R4793.
[27] W. Han, K. Pi, K.M. Mccreary, Y. Li, J.J.I. Wong, A. Swartz, R. Kawakami, Tunneling spin injection into single layer graphene, Phys. Rev. Lett. 105 (16) (2010), 167202.
[28] A. Avsar, T. Yang, S. Bae, J. Balakrishnan, F. Volmer, M. Jaiswal, Z. Yi, S.R. Ali, G. Güntherodt, B. Hong, et al., Toward wafer scale fabrication of graphene based spin valve devices, Nano Lett. 11 (6) (2011) 2363–2368.
[29] M.V. Kamalakar, A. Dankert, P.J. Kelly, S.P. Dash, Inversion of spin signal and spin filtering in ferromagnet—hexagonal boron nitride-graphene van der waals heterostructures, Sci. Rep. 6 (2016) 21168.
[30] B. Zhao, B. Karpiak, D. Khokhriakov, A. Johansson, A.M. Hoque, X. Xu, Y. Jiang, I. Mertig, S.P. Dash, Unconventional chargecspin conversion in weyl-semimetal wte2, Adv. Mater. 32 (38) (2020) 2000818.
[31] B. Zhao, D. Khokhriakov, Y. Zhang, H. Fu, B. Karpiak, A.M. Hoque, X. Xu, Y. Jiang, B. Yan, S.P. Dash, Observation of charge to spin conversion in weyl semimetal wte_2 at room temperature, Phys. Rev. Research 2 (2020), 013286.
[32] Y.K. Luo, J. Xu, T. Zhu, G. Wu, E.J. McCormick, W. Zhan, M.R. Neupane, R.K. Kawakami, Opto-valleytronic spin injection in monolayer mos_2/few-layer graphene hybrid spin valves, Nano Lett. 17 (6) (2017) 3877–3883.
[33] M. Gmitra, J. Fabian, Graphene on transition-metal dichalcogenides: a platform for proximity spin-orbit physics and optospintronics, Phys. Rev. B 92 (15) (2015), 155403.
[34] A. Avsar, D. Unuchek, J. Liu, O.L. Sanchez, K. Watanabe, T. Taniguchi, B. Özyilmaz, A. Kis, Optospintronics in graphene via proximity coupling, ACS Nano 11 (11) (2017) 11678–11686.
[35] D. Khokhriakov, A.M. Hoque, B. Karpiak, S.P. Dash, Gate-tunable spin-galvanic effect in graphene-topological insulator van der waals heterostructures at room temperature, Nat. Commun. 11 (2020) 3657.
[36] B. Karpiak, A.W. Cummings, K. Zollner, M. Vila, D. Khokhriakov, A.M. Hoque, A. Dankert, P. Svedlindh, J. Fabian, S. Roche, S.P. Dash, Magnetic proximity in a van der waals heterostructure of magnetic insulator and graphene, 2D Mater. 7 (1) (2020), 015026.
[37] D. Wu, X. Cao, S. Chen, L. Tang, Y. Feng, K. Chen, W. Zhou, Pure spin current generated in thermally driven molecular magnetic junctions: a promising mechanism for thermoelectric conversion, J. Mater. Chem. 7 (32) (2019) 19037–19044.
[38] G. Kresse, J. Furthmüller, Efficient iterative schemes for ab initio total-energy calculations using a plane-wave basis set, Phys. Rev. B 54 (1996) 11169–11186.
[39] G. Kresse, J. Hafner, Ab initio molecular dynamics for liquid metals, Phys. Rev. B 47 (1993) 558–561.
[40] H.J. Monkhorst, J.D. Pack, Special points for brillouin-zone integrations, Phys. Rev. B 13 (1976) 5188–5192.
[41] J.P. Perdew, K. Burke, M. Ernzerhof, Generalized gradient approximation made simple, Phys. Rev. Lett. 77 (18) (1996) 3865.
[42] J. Taylor, H. Guo, J. Wang, Ab initio modeling of quantum transport properties of molecular electronic devices, Phys. Rev. B 63 (24) (2001), 245407.
[43] J. Taylor, H. Guo, J. Wang, Ab initio modeling of open systems: charge transfer, electron conduction, and molecular switching of a c_{60} device, Phys. Rev. B 63 (2001), 121104.
[44] For details of the nanodcal quantum tranpsort package. http://hzwtech.com/.
[45] L. Kleinman, D. Bylander, Efficacious form for model pseudopotentials, Phys. Rev. Lett. 48 (20) (1982) 1425.
[46] L. Zhang, K. Gong, J. Chen, L. Liu, Y. Zhu, D. Xiao, H. Guo, Generation and transport of valley-polarized current in transition-metal dichalcogenides, Phys. Rev. B 90 (19) (2014) 195428.
[47] J. Chen, Y. Hu, H. Guo, First-principles analysis of photocurrent in graphene *pn* junctions, Phys. Rev. B 85 (2012), 155441.
[48] Y. Xie, L. Zhang, Y. Zhu, L. Liu, H. Guo, Photogalvanic effect in monolayer black phosphorus, Nanotechnology 26 (45) (2015) 455202.
[49] J. Chen, L. Zhang, L. Zhang, X. Zheng, L. Xiao, S. Jia, J. Wang, Photogalvanic effect induced fully spin polarized current and pure spin current in zigzag sic nanoribbons, Phys. Chem. Chem. Phys. 20 (41) (2018) 26744–26751.
[50] L.E. Henrickson, Nonequilibrium photocurrent modeling in resonant tunneling photodetectors, J. Appl. Phys. 91 (10) (2002) 6273–6281.
[51] Y. Son, M.L. Cohen, S.G. Louie, Half-metallic graphene nanoribbons, Nature 444 (7117) (2006) 347–349.
[52] E. Kan, Z. Li, J. Yang, J.G. Hou, Will zigzag graphene nanoribbon turn to half metal under electric field, Appl. Phys. Lett. 91 (24) (2007) 243116.
[53] V.I. Belinicher, B. Sturman, The photogalvanic effect in media lacking a center of symmetry, Sov. Phys. Usp. 23 (3) (1980) 199–223.
[54] S.M. Young, F. Zheng, A.M. Rappe, Prediction of a linear spin bulk photovoltaic effect in antiferromagnets, Phys. Rev. Lett. 110 (2013), 057201.
[55] X. Tao, P. Jiang, H. Hao, X. Zheng, L. Zhang, Z. Zeng, Pure spin current generation via photogalvanic effect with spatial inversion symmetry, Phys. Rev. B 102 (2020), 081402.